Title
ELASTIC SCATTERING OF 48-MEV ALPHA PARTICLES BY HEAVY NUCLEI

Author
Ellis, Robert E.

Publication Date
1955-08-22

UCRL 3114

UNIVERSITY OF
CALIFORNIA

Radiation
Laboratory

ELASTIC SCATTERING OF 48-Mev ALPHA PARTICLES BY HEAVY NUCLEI

DISCLAIMER

UCRL-3114
Physics Distribution

UNIVERSITY OF CALIFORNIA

Radiation Laboratory
Berkeley, California

Contract No. W-7405-eng-48

ELASTIC SCATTERING OF 48-Mev ALPHA PARTICLES BY HEAVY NUCLEI

Robert E. Ellis

(Thesis)

August 22, 1955

Printed for the U. S. Atomic Energy Commission

Contents

ELASTIC SCATTERING OF 48-Mev ALPHA PARTICLES BY HEAVY NUCLEI

Robert E. Ellis

Radiation Laboratory
University of California
Berkeley, California

August 22, 1955

ABSTRACT

The angular distributions of alpha particles scattered elastically from Ag, Au, and Pb targets have been measured. Deviations by three to four orders of magnitude from pure Coulomb scattering have been observed beyond the forward angles. In addition, some regular structure appears in these distributions, but the main features can be described by an exponential fall-off between 25° and 90°.

By fitting the data with a simple modification of Blair's scattering theory, it has been possible to determine interaction radii. Nuclear radii have been derived which are in agreement with those found from medium-energy nucleon scattering.

I. INTRODUCTION

In general, scattering theory is concerned with the interpretation of angular distributions with respect to the character of nuclear forces and the potentials from which they arise; the organization of the nucleons in the nucleus and the charge distribution; and, with extremely high-energy bombarding particles, perhaps the actual substructure of the nucleons themselves.

The earliest scattering experiments using alpha particles[1] served to establish the atomic model and to give some information about the nuclear size and about nuclear forces. As accelerators were developed, even though it became possible to make alpha particles which could penetrate the Coulomb barrier for the heavier nuclei, the emphasis in scattering naturally tended toward the use of the "simpler" particles - the neutron, proton, and deuteron. The alpha particle is not considered as desirable a bombarding particle, since its own internal structure tends to complicate the interpretation of scattering data. To the extent that the alpha-particle interaction with heavy nuclei depends on the electric forces alone, the problem has been completely described, both classically and in terms of quantum theory.

Many authors[2] have discussed the partial-wave analysis of scattering, in which the scattered waves are analyzed on the basis of the angular momenta associated with different partial waves, and the resulting angular distribution of particles is explained as the interference associated with the interaction of these components. The theoretical construction of such angular distributions is predicated on the possibility of determining the phase shifts associated with the various possible angular momentum values.

Recently, in order to explain the variation of alpha-particle elastic scattering with energy,[3] Blair[4] proposed a semiclassical scattering model which requires only the use of the well-known phase shifts that appear in the Coulomb interaction. Assuming a well-defined radius for both the target nucleus and the incident alpha particle, he derives the following angular distribution for elastically scattered

alpha particles, relative to pure Coulomb scattering (See Appendix I):

$$\frac{\sigma}{\sigma_c} = \left| -ie^{-in\ell n \sin^2\frac{\theta}{2}} - \frac{\sin^2\frac{\theta}{2}}{n} \sum_{\ell=0}^{\ell'} (2\ell+1) W_\ell e^{2i(\delta_\ell - \delta_0)} P_\ell(\cos\theta) \right|^2 , \quad (1)$$

where ℓ' satisfies the relation

$$\ell'(\ell'+1) = (E - E_c)\frac{2MR^2}{\hbar^2} \quad (2)$$

with $$E_c = \frac{ZZ'e^2}{R} .$$

Here ℓ' refers to the orbital angular momentum of a particle, in the center-of-mass system, of reduced mass M, energy E, and velocity v; E_c is the Coulomb energy at the classical turing point; R is the sum of target radius and alpha-particle radius; Ze is the charge of the target nucleus and Z'e is the charge of the alpha particle; and W_ℓ is the weight given to the absorption of the ℓ^{th} partial wave. The Coulomb phases obey the relation

$$e^{2i(\delta_\ell - \delta_0)} = \frac{\ell + in}{\ell - in} \; e^{2i(\delta_{\ell-1} - \delta_0)} ,$$

and $$n = \frac{ZZ'e^2}{\hbar v} .$$

The first term in Eq. (1) represents the Coulomb scattering amplitude, and the second term the interaction with the nucleus of alpha particles with $\ell \leq \ell'$. Blair assumes that all these partial waves with $0 \leq \ell \leq \ell'$ vanish because the trajectory is such that the alpha particle is completely absorbed by the nucleus, excites the nucleus, and is lost to elastic scattering, or is broken up into smaller components. Thus $W_\ell = 1$ (complete absorption) for $0 \leq \ell \leq \ell'$. If the nucleus and alpha particle do not overlap, the outgoing ℓ^{th} partial wave associated with the alpha particle is considered to have purely Coulomb phase characteristics; $W_\ell = 0$ (no absorption) for $\ell > \ell'$. This model is referred to as the "sharp cutoff" model because complete nuclear absorption ends and complete Coulomb scattering begins at a well-defined distance from the scattering center. The model neglects barrier penetration and reflection from the nuclear potential, and takes no account of the mean free path of the alpha particle in nuclear

matter. Although this theory reproduces the general qualitative features of observed angular distributions – namely, a rise followed by a sharp fall-off – the theoretical curves show a diffraction pattern with large-amplitude oscillations which is not observed. This last effect is presumably due to the sharp radial cutoff of the Blair theory.

Other investigators[5] have attempted to improve the model in a simple way, by taking $W_\ell = 1$ for $0 \leq \ell < \ell'$, $W_\ell = 0.5$ for $\ell = \ell'$, and $W_\ell = 0$ for $\ell > \ell'$. This "fuzzy" model tends to smooth out the transition region of interaction, and substantially improves the fits to the data at 22 Mev. This fitting results in a determination of the interaction radii, which are found to be larger than the generally accepted values.

Recently, Porter[6] has proposed a classical interpretation of the dependence of the ratio of observed differential cross section to the Coulomb cross section on the classical apsidal distance, D (the distance of closest approach). His description embodies the principle that the scattered intensity, as a function of apsidal distance (and, therefore, of the incident energy and angle of scattering) arises entirely from absorption along the Coulomb orbit. He defines the ratio of observed to Coulomb cross section in terms of a transmission factor T, which is equal to the fraction of the incident beam that is scattered at a given angle, relative to the Coulomb scattering. T has the form

$$T = \exp\left(-\int \frac{dx}{\ell(x)}\right),$$

where $\ell(x)$ = mean free path of the alpha particle as a function of the position coordinate x along the path. Assuming straight-line paths through the nucleus, he obtains the expression

$$T = \exp\left(-2\frac{R}{\ell_o}\, h\left[\xi, \delta\right]\right),$$

where $h\left[\xi, \delta\right] = \int_{\xi}^{\infty} dv (v^2 - \xi^2)^{1/2} \operatorname{sech}^2\left(\frac{v-1}{\delta}\right)$

and $\xi = D/R$, where R = interaction radius, the sum of nuclear and alpha-particle radii;

$v = r/R$, where r = distance from nuclear center to the center of the alpha-particle;

$\delta = d/R$, where d = measure of the thickness of the diffuse edge of the nucleus;

l_o = mean free path of the alpha-particle near the center of the nucleus.

From data previously available[3,5,7] he deduces values of $R/l_o \sim 3$ or 4 for alpha particles, $\delta \sim 0.2$, and $d \sim 2 \times 10^{-13}$ centimeters, indicating that the nucleus is opaque to alpha particles except near the edge of the nucleus, in the diffuse region. The slight rise of T above the value of one for small angles, and the structure in the observed distributions which probably arises from wave-mechanical interference effects, are not explained on this model.

Unpublished calculations by Ford and Wheeler[6,7] on the elastic scattering of alpha particles are based on a model in which the "rim" of the nucleus is transparent to the alpha particles. Best agreement between experiment and theory on this model is for large energy and scattering angle for the alpha particle.

In addition to the models of Blair and Porter, an optical model with real and imaginary parts to the potential could be used to analyze elastic alpha-particle scattering. Comparisons of this model with experiment may be related to the magnitude and shape of both real and imaginary parts of a nuclear potential, as well as an interaction radius. In general, the real potential (scattering potential) is considered to have a depth of ~45 Mev for a nucleon, and the imaginary part of the potential (absorption) varies as a function of the incident energy, being smaller for low and high energies of the incident particle and having a maximum value for some intermediate energy--for neutrons or protons it may be ~9 to 10 Mev deep at incident energies of 20 Mev.[8,9]

Other investigators[3,5,7] have studied elastic alpha-particle scattering, both from the point of view of energy dependence and angular dependence of the cross section. The reported investigations were carried out at somewhat lower energies (13 Mev to 44 Mev) than those reported here. They show a pronounced deviation from Coulomb

scattering at relatively small angles of scattering, and the ratio of observed to Coulomb cross section is essentially an exponentially decreasing function of angle over a wide range of angles beyond the point at which the break with Coulomb scattering is observed.

The purpose of the experiments described here was to extend these investigations, both as to theory and experiment. For comparison's sake, the heavy target nuclei of silver, gold, and lead were concentrated on, as it would be interesting to compare the results at higher bombarding energy with those obtained at lower energies.

II. EXPERIMENTAL METHOD

A. General Procedure

A schematic diagram of the experimental arrangement is shown in Fig. 1. The 48-Mev alpha-particle beam of the 60-inch cyclotron at the Crocker Laboratory was brought out through the water shielding and impinged on a target located at the center of a large vacuum scattering chamber. The scattered particles were detected by a triple-coincidence proportional counter telescope. At each angular setting of the detector, the number of alpha particles elastically scattered during a convenient time interval was observed with the telescope and normalized against the total charge collected by a Faraday cup located behind the chamber. The detected particles were selected by placing absorbers in front of the counter and requiring a preset minimum pulse height in each counter chamber. In this way, the relative elastic-scattering cross section was obtained as a function of the laboratory angle.

B. The Alpha-Particle Beam

A deflected beam of 40 microamperes of 48.2-Mev alpha particles was internally collimated by a 1/8-inch slit probe. The beam emerging from the cyclotron target port was passed through a short iron presnout, 6 inches long, and then through a long iron snout 60.5 inches long. The snouts provided a relatively field-free region for the purpose of extracting the beam through the fringing

field of the cyclotron magnet. The beam traveled the remaining 15 feet through a 1.5-inch-diameter brass pipe to a point outside the cyclotron water-wall shielding, where the scattering chamber was located.

After the beam entered the brass pipe it passed through a strong-focusing quadrupole-type magnetic lens and was focused at the target in the scattering chamber in a spot 0.25 inch in diameter. A collimating section 18 inches long, containing three carbon collimators, was located externally to the chamber, collimating the beam to about a 1/8-inch spot at the target. The maximum beam easily attainable at the entrance to the carbon collimators was 6 microamperes of 48.2-Mev alpha particles. It might be mentioned that essentially the same strength of beam of protons or deuterons was also available with the same focusing arrangement. The maximum beam at the target, using the 1/8-inch collimating system, was about 0.6 microampere at a reasonable cyclotron oscillator power.

In order to reduce background for large-angle measurements, the collimator section was removed and the strong-focused beam was used without any collimation except that afforded by a set of carbon slits arranged on the cyclotron side of the strong-focusing magnets.

C. Alignment Procedure

The deflected cyclotron beam was initially centered at the cyclotron target port by adjusting the position of the internal slit probe mentioned above. It was then centered at the end of the long iron snout by position adjustments of the snout and application of external magnetic shims at the presnout, and next at the end of the 1.5-inch brass beam duct (without the strong-focusing lens turned on) using nuclear emulsion burns. A fluorescent plate and remote telescopic observation, along with nuclear emulsion burns, were then used to center the focused beam in the exit aperture of the beam duct with the magnetic lens turned on.

With the 36-inch scattering chamber in position, the chamber collimating slits were aligned on the center of the beam-duct aperture, as well as on the center of the iron snout, by means of a telescope placed at the exit port of the chamber. It was then possible

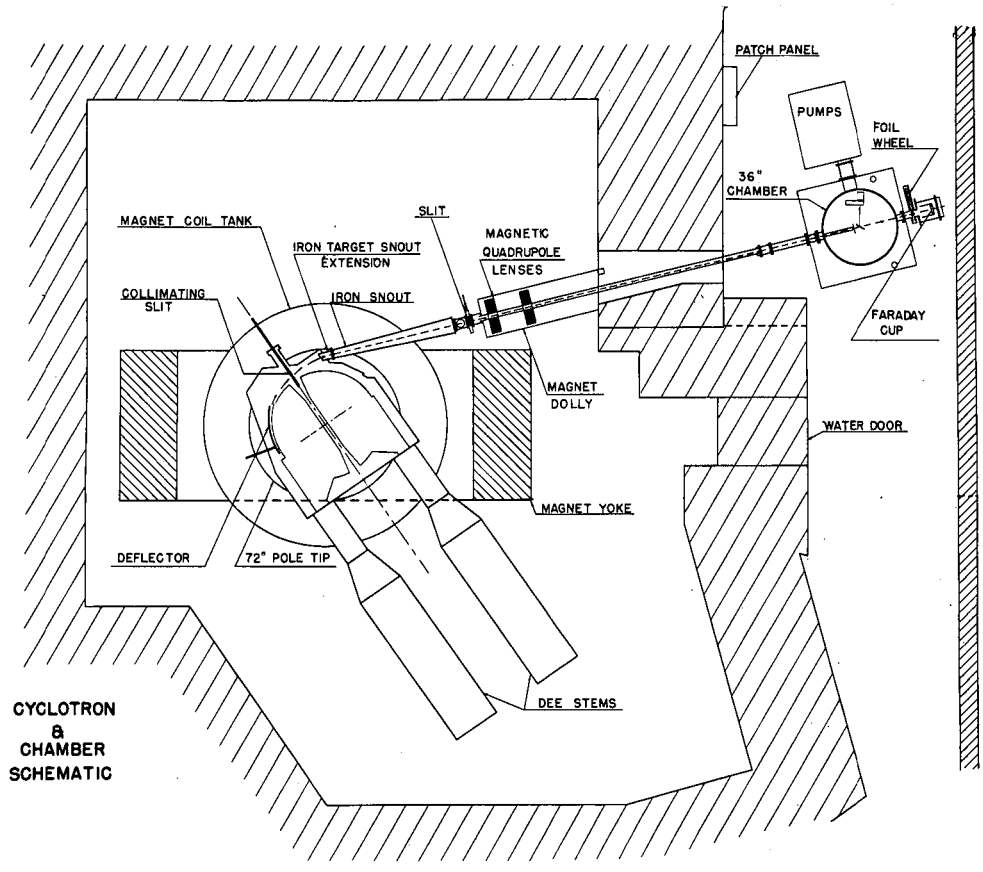

Fig. 1. Schematic diagram of experimental arrangement.

to put a vacuum on the system and take nuclear emulsion or scotch tape burns at a point very near the target position and on the 0^{o}-180^{o} line of the chamber. The spot thus obtained was centered at that point by suitable fine adjustments of the scattering-chamber position. The alignment by this method was then completed by taking a nuclear emulsion burn at the exit port of the scattering chamber.

The optical method and burn method were subsequently checked by comparing the counter yield of counts for a given position on one side of the chamber with the yield at a corresponding point on the opposite side (scattering is cylindrically symmetric about the beam direction). Such methods always agreed to within 0.5^{o}. An additional check was made by running the proportional counter through the zero forward direction of the beam, at reduced beam, and noting the counts as a function of angular position of the counter. It is believed this method was reliable to within 0.5^{o} when the chamber collimators were used, even though the large decrease in beam intensity from normal operating conditions might change the position of the intense portion of the strong-focused beam within the limits of the diameter of the collimated spot. When no chamber collimators were used, the magnitude of the normal beam necessitated detuning of cyclotron parameters (oscillator power, arc current, etc.), including the deflector in some cases, so that the most reliable criteria of beam direction were assumed to be a combination of those previously mentioned.

The strong-focused beam spot at the target was essentially 0.25 inch in diameter. After alignment, the strong-focusing magnet current was never varied, for the shape of the spot depended strongly on that current.

D. Scattering Chamber, Vacuum System, and Target Mechanism

The scattering chamber used has been described by G. Fischer.[10] It is 36 inches in internal diameter and 13 inches deep, and contains a rotating table, remotely controlled by selsyn motors, upon which counters and associated equipment can be accurately located with respect to the center of the chamber. Rotating control was accurate to less than 0.5^{o}. High-voltage vacuum insulators and coaxial leads

were brought in through the center of the rotating table. Means of leveling, and fine adjustments of position, vertically and horizontally, were provided which were independent of the supporting base. Suitable glass observation ports and access ports were provided, as well as stainless steel window ports extending around portions of the side of the chamber for use with external detectors. The dimensions of the counter used in these experiments permitted measurements of the scattering at angles between 7° and 170°.

A portable vacuum system consisting of a Kinney forepump and a refrigerated 6-inch oil diffusion pump were designed for specific use with the scattering chamber. A vacuum of approximately 3×10^{-4} mm Hg was normally obtained with the system, although at times somewhat lower vacuums were attained.

The target mechanism provided for the mounting of several targets, arranged in a vertical plane, so that any one of the targets might be positioned in the beam vertically and azimuthally, remotely controlled by selsyns. Positioning was found to be accurate to within about 0.25° azimuthally.

E. Beam Monitoring and Beam Energy Determinations

A cylindrical brass Faraday cup, maintained in a separate vacuum compartment with its own diffusion pump, was located on the beam-exit port of the scattering chamber. Two opposed C-shaped magnets (Alnico III) were located at the rear of the cup and provided a uniform field of about 200 gauss for prevention of secondary electron loss occasioned by the beam's striking the beam-stopping plate. Suitable coaxial leads permitted transmission of the beam current to a 100% negative feedback electrometer located in the counting area.

The precision capacitors used in conjunction with the integrating electrometer were calibrated against precision capacitors of the same nominal values. These in turn had been calibrated against a 1.0-microfarad condenser certified by the Bureau of Standards. Capacitors used in integrating the beam were calibrated for each run, and it is believed that their values are correctly known to within 1%. The voltage on the integrating condensers was measured during a run by a Speedomax recorder. The linearity of response of the

recorder and electrometer scale factors were checked for each run and any variation in values thus obtained was taken into account. It is thought that the voltages read from the recorder are accurate to 0.5%.

Between the scattering chamber and the Faraday cup chamber was an absorber foil changer consisting of a vacuum chamber with two twelve-position foil wheels. Each wheel was controlled independently and remotely so that suitable combinations of foils provided a means of measuring the primary cyclotron beam energy without the necessity of turning off the cyclotron. This was very desirable because of the warm-up period of the cyclotron, during which, for a period of about fifteen or twenty minutes, the beam energy gradually increased (i.e., the oscillator frequency increased as a function of warm-up time) to its steady-state value.

Other methods of determining beam energy were employed, but the least time-consuming way was that of reading the voltage across a suitable resistor, with the integrating electrometer mentioned above, and plotting this voltage automatically by means of a Speedomax recorder as a function of absorber inserted into the beam. This method actually plotted automatically the integral number-range curve of the primary beam, from which the mean range was readily determined. The principal disadvantage of the method arose from beam fluctuations during the run, but experience indicated that a reasonably steady beam gave results reliable to within about 1 mg/cm^2 of aluminum, or about 0.5% of the range of the 48-Mev alpha particles. The beam range determination was made at the beginning and end of each day's run.

Further monitoring of the beam for the purpose of tuning cyclotron parameters was accomplished by the use of a NaI crystal scintillation counter (using a Du-Mont 6292 photomultiplier tube), placed externally to the scattering chamber at a forward angle of 20° and coupled by a cathode follower-linear amplifier-attenuator circuit to a counting-rate meter located in the cyclotron control room. The signal from this monitor also drove a discriminator and scaler and thus could be used as a further check on the operation of the primary

monitoring circuit.

F. Counter Characteristics

A triple-coincidence proportional-counter telescope was used as a detector. This counter consisted of three chambers, each with a sensitive volume 0.5 inch deep and approximately 2 square inches in area. Each chamber contained one central ground wire and two collector wires at positive high voltage, all wires being 3-mil polished stainless steel (see Fig. 2).

In the original design, the counter chambers contained four high-voltage collecting wires and three ground wires arranged alternately 0.25 inch apart, for the purpose of providing an approximately cylindrical electrostatic field about each collector wire. With a well-collimated source of Cm^{242} alpha particles, rather exhaustive tests were made which indicated that the least deviation from a mean pulse height in a sensitive volume about 1.5 inches in diameter was obtained with the two outer collector wires and ground wires removed, and the remaining two collector wires located at a distance of 5/16 inch from the central ground wire.

Each counter chamber was individually tested in a constant-flow test chamber with a mixture of A-CO_2 gas, in proportions of 96% to 4%, which was further purified by passing through a copper cooling-coil system immersed in a slush of dry ice and acetone.

The results of the counter tests indicated that within a circle 1.5 inches in diameter, centered on the counter, the pulse-height distribution at any given point varied from 6% to 8% full width at half maximum, whereas the peak pulse height varied from point to point by ± 3% from the average. The "fold" of these distributions gave a gaussian distribution with width at half maximum of 10.4%.

As it was found that counter voltages exceeding about 1550 volts caused a broadening of the distribution of pulses from the test source, a motor-driven wire-polishing machine* was constructed in which six wires could be polished simultaneously. Microscopic comparison of the polished wires with unpolished ones indicated

---

* Constructed by W. M. Brower, Dept. of Physics, University of California

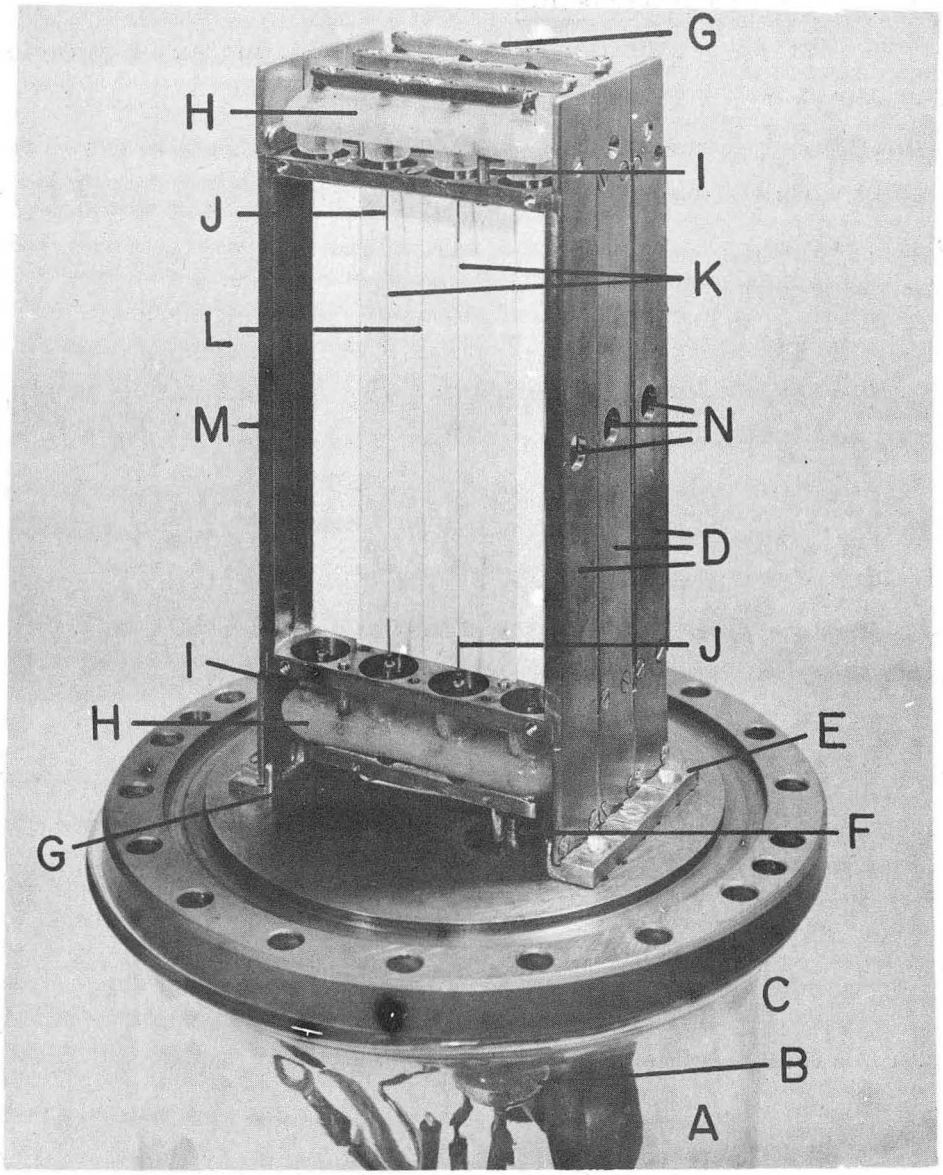

Fig. 2. Proportional counter chamber assembly.
A-Vacuum valve. B-Kovar insulators for high-voltage leads. C-Vacuum lid, forming base for counter. D-Three counter chambers. E-Aligning bases for counter chambers. F-High voltage lead. G-High-voltage bus bar, which also provides means of holding collector wires in place. H-Precision glass-Kovar insulators. I-Kovar support stud for insulator. J-23-gauge hypodermic defining needles which are mounted in holes in 0-80 screws, in turn screwed into Kovar tubes of the glass insulators. K-0.003-inch stainless steel polished collector wires. L-0.003-inch stainless steel ground wire. M-Brass counter frames, individually demountable from aligning base. N-3/16-inch holes for entrance of source particles into sensitive volume of the counter. NOTE: The front foil has been removed, and a sheet of paper placed in front of the foil between chambers 1 and 2, in order to more clearly define the position of the wires.

ZN-1311

a measurable gain in smoothness. The actual improvement in pulse-height distribution resulting from this operation was not determined, but it is reasonable to assume that variations in electron multiplication as a function of position along the wires, caused by higher electrostatic field gradients in the vicinity of sharp points, may have been reduced to some extent.

Because the detection of particles at small scattering angles was desirable, the counter was constructed in such a way that the sensitive volume was very nearly the same (at least, in the lateral dimension) as the volume of the outer vacuum cover, thus permitting the closest approach to the forward direction without interfering with the primary beam collection.

The internal insulation of the counter was provided by specially cast glass insulators with threaded Kovar metal tubes inserted to provide means of fastening the insulators to the brass chamber frames and also for holding the hypodermic needles which were used to define the sensitive volume. All insulators and wires were mounted in place with screws. Wire tension was obtained by applying the required tension at the time of installation.

For purposes of testing and calibration three Cm^{242} alpha sources were located on the side of the counter vacuum cover, separated from the sensitive volume by 0.25-mil aluminum foils. A remotely controlled sliding shutter, moved by means of small solenoids, was installed between sources and foil so that the pulses obtained might be observed at will. Because of their location, the pulse-height distributions from these sources had a low-pulse tail, but their mean pulse height could be used as a relative measure of counter characteristics as a function of time during a run, as well as for prerun testing of counting equipment.

Because the proportional counter was to be used in a long-range program for the detection of alpha particles, deuterons, protons, and possibly other charged particles, its pulse-height distribution characteristics were of particular interest. Pulse-height distributions of from about 10% to 15% (Fig. 3) have been observed for 48-Mev alpha particles, for settings of discriminator bias below

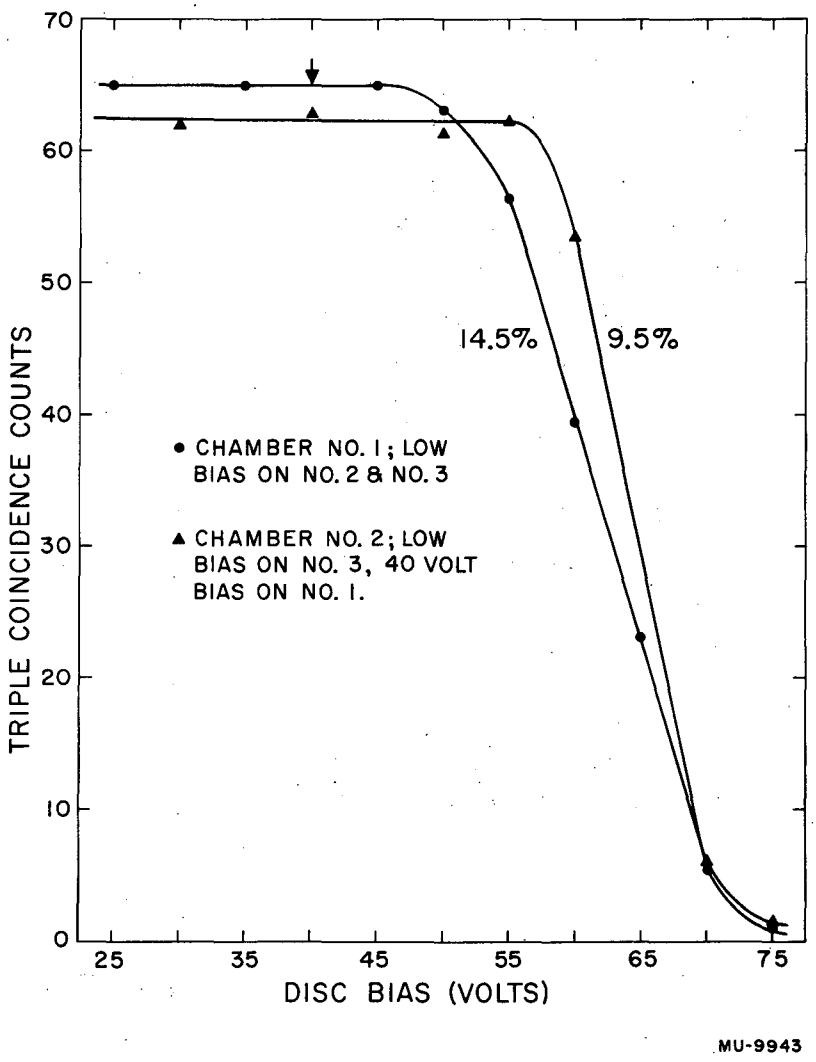

Fig. 3. Integral pulse-height distribution curves obtained with the proportional counter telescope.

the "knee" of the bias curves. The "width" of the pulse-height distribution is that pulse height interval which contains one-half the observed pulses, as defined by Rossi and Staub.[11]

For particles that are detected in the counter, the deuteron-to-proton ratio of pulse heights in the first chamber should be about 1.3, and for alpha-particles versus protons, about 4.

G. Electronics and Associated Controls

A block diagram of a typical electronics setup is shown in Fig. 4.

Positive high voltage was supplied to each chamber of the proportional counter separately. A single, well-regulated 2-kv high-voltage supply was used for all three chambers, with the convenient feature that individual adjustments for each of four output channels was provided, with sufficient latitude in adjustment that the pulse height in all three chambers could easily be adjusted to the same value for a given absorber setting. A switch box for the outputs enabled one to read accurately the voltage on any chamber by means of a Leeds-Northrup potentiometer. The voltage from this regulated supply was observed not to vary over 1 or 2 volts out of 1500 volts for a period of six or seven days.

Line voltage regulation was obtained with a 2.5-kva Stab-I-Line voltage regulator. This 120AC regulated voltage was available for linear amplifiers and variable gate-variable delay discriminator units. Sola voltage regulators supplied regulated voltage to other components such as scalers, etc. All equipment racks were refrigerated, and tests indicated a temperature regulation of approximately 1°C during a twenty-four hour period, with short-time regular periodic variations, due to thermostatic action, of 2° about a mean value of 19° C.

Nominally square delay-line-clipped counter pulses of 1 microsecond duration were used, with a rise time of about 0.2 microsecond. Preamplifiers, suspended from the bottom of the scattering chamber, provided a gain of about seventy-five to the linear amplifiers. This increased gain (at some small sacrifice of pulse rise time) was introduced in order to avoid high counter voltages.

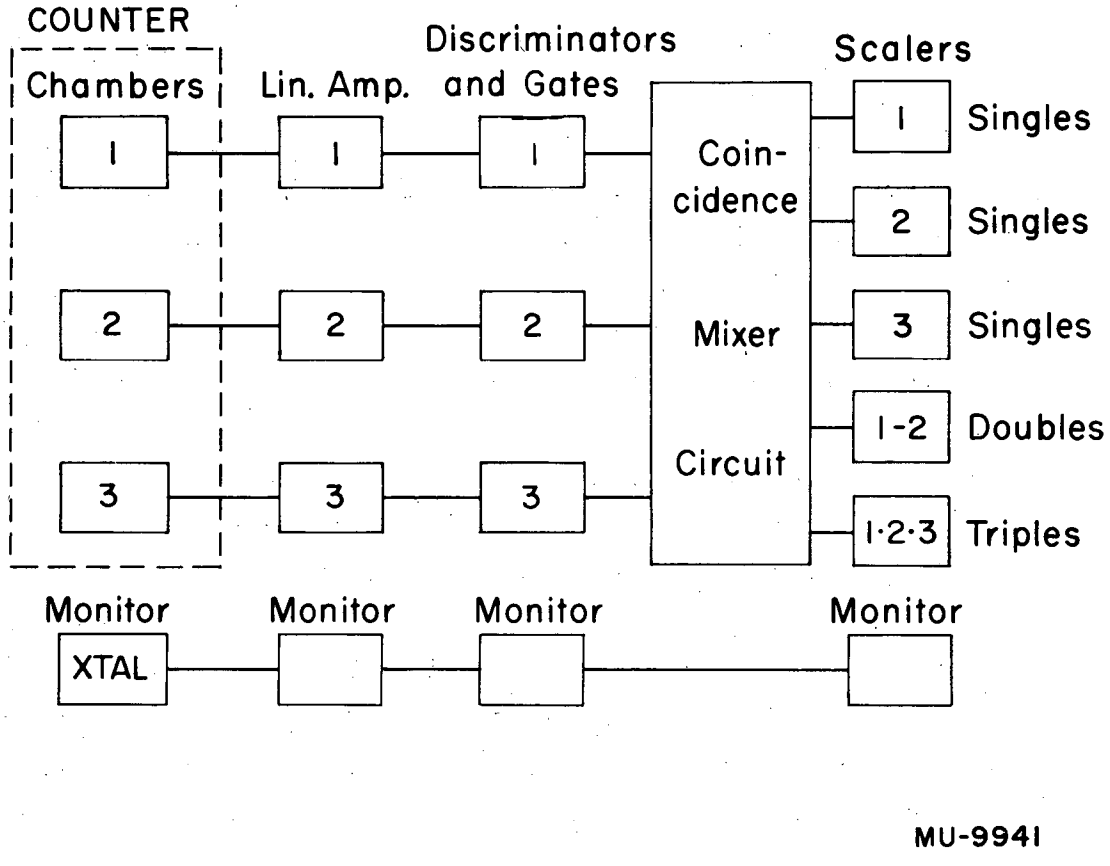

Fig. 4. Block diagram of the electronics.

Jitter in the formation of the variable gates as a result of differences in electron collection time in different counter chambers, and electronics effects, was less than 0.5 microsecond. Counting rates were always determined by finding the extent of the beam plateau (region in which counts per microcoulomb of integrated beam, as a function of beam intensity, remained essentially constant). In this way, loss of counts because of dead time in counter and discriminators, or loss of register counts in the scalers, was avoided.

H. Measurement of the Angular Distributions

The elastic alpha particles were detected in the following manner: At some convenient angular setting of the counter telescope, sufficient absorber was inserted so that the elastic alpha particles stopped in a given counter chamber, say No. 1 (Fig. 5) The counter voltage and the amplifier gain for that chamber were set for pulses that just reached saturation without overloading. This procedure was repeated for each of the other chambers. Discriminator curves were run for the pulses from each of the chambers at an absorber setting 20 mg/cm^2 below the value that had produced the peak pulse heights. The biases were then set so that chambers No. 1 and No. 2 could detect an alpha particle with 20 mg/cm^2 of residual range or less. Chamber No. 3 had its bias set very low, so that it could detect any pulse above the amplifier noise. The coincidence circuits monitored both 1-2 coincidences (doubles) and 1-2-3 coincidences (triples). Differential range spectra were run by plotting doubles minus triples against absorber thickness for a fixed amount of collected charge in the Faraday cup. The elastic peak showed up well and its width could be accounted for by the spread in incident beam energy, range straggling, the range "bite" of the counter, and the target thickness. At absorber settings just below the peak, the doubles rate was essentially flat, and represented the integral of the differential elastic peak. The desired angular distributions, then, were made by measuring these double coincidences as a function of angle, normalized to the charge collected by the Faraday cup. Each point was multiplied by $\sin^4\theta/2$ to give

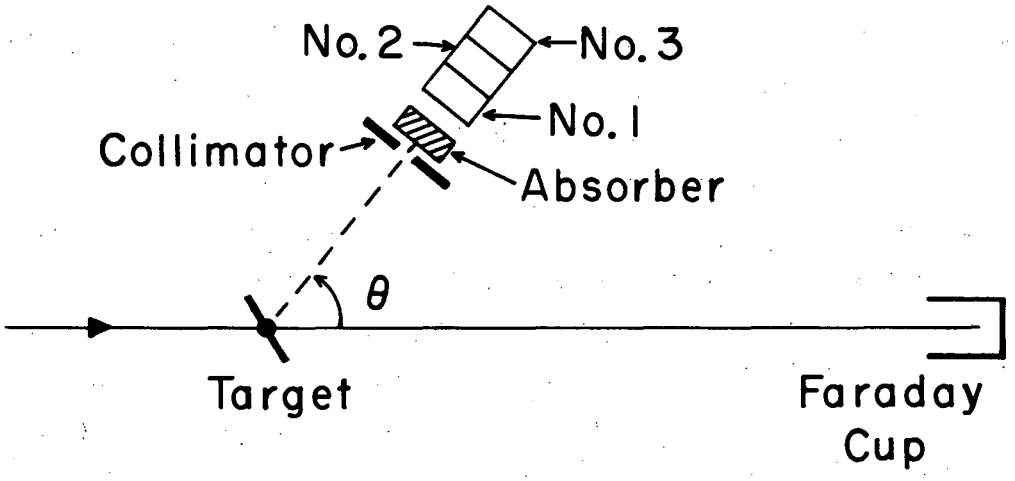

Fig. 5. Schematic diagram of the counter arrangement.

the ratio to Coulomb scattering. Good reproducibility was observed from run to run, and many of the data were run several times in order to verify structure in the distributions. Runs at different beam levels or between different angular regions always included overlapping measurements, to insure that no substantial error in normalization remained undetected.

It was, of course, also possible to integrate numerically the differential spectrum at each angle. Comparison of the two methods always gave very good agreement for a reasonable value of the range "bite" of the counter (the thickness of the range foil plus about one-half the thickness of the second chamber, depending on bias settings in the second and third counter chambers).

The differential spectrum was run at angles up to 75° in making this check. The good agreement between the differential and integral methods gave confidence that the quantity being measured was actually the elastic-scattering cross section. Typical curves of the integral and differential spectra are shown in Fig. 6.

I. Background

At each angle, data were taken with the target out, to account for background. At regular intervals complete differential range spectra were run in order to determine the background level. It turned out that the background was insignificantly low at angles out to about 50°. Beyond, the elastic peak was found in the midst of a general background of charged particles which appeared at absorber settings both above and below that of the elastic alpha particles. For the wider angles, the doubles rate was determined both immediately above and below the elastic peak for target out and target in, and this background was taken into account.

To reduce background at the chamber, the three carbon collimators, located at the scattering chamber, were removed. Adjustable carbon slits on the cyclotron side of the strong-focusing magnet (see Fig. 1) were set to 0.3 inch or less. This markedly reduced both the target-out background and the target-in doubles count above the elastic peak. The strong-focused beam was then

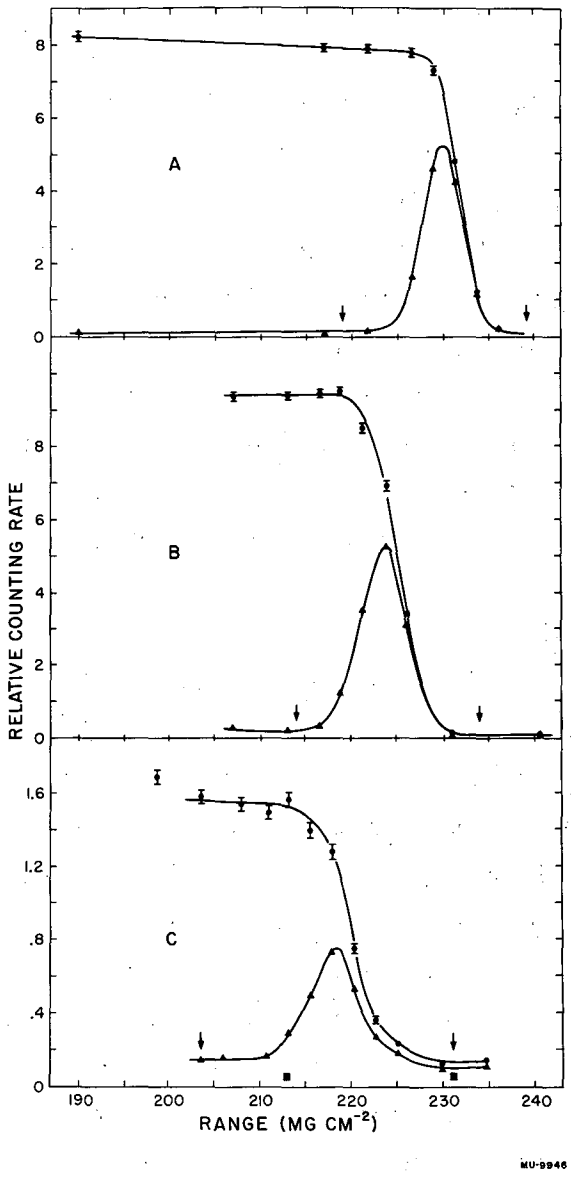

Fig. 6. Typical integral and differential range spectra. 6A is for Au at 45°, 6B is for Ag at 30°, and 6C is for Pb at 75°.

0.25 inch in diameter at the target position. All of the data on Pb were run without the chamber collimators, and for forward angles, the adjustable carbon slits just before the strong-focusing magnet were closed to about 0.05 inch.

One possible source of error might have arisen if inelastic alpha particles with small energy losses had been counted in significant numbers. It is not likely that this happened, since the observed data fitted the Coulomb scattering at the forward angles (up to 20°) and there was essentially no such background in plots of the differential spectra.

A calculation indicates that alpha particles scattered elastically from any residual carbon or oxygen on the targets would not be detected beyond about 15°. Between 7° and 15° any such contaminant effect would be small compared to the large cross section of the target

J. Resolution

The cyclotron beam was collimated by means of adjustable carbon slits to less than 0.3 inch in width before it entered the strong-focusing lens system. When focused at the target position in the usual 0.25-inch-diameter spot, it was considered to be a parallel beam of particles. Because the target was always maintained at 45° to the plane perpendicular to the beam direction, the scattered particles emerged from an elliptical spot. With multiple scattering in the target, the size and shape of the target spot, and the size of the counter collimator, taken into consideration, the angular resolution was determined by a fold of the functions representing these quantities. The width at half maximum was $\pm 1^{\circ}$ for the least favorable case in which a Pb target was bombarded without the 1/8-inch carbon collimators mounted in the beam duct just outside the scattering chamber.

K. Estimate of error

The ratio σ/σ_c of the observed differential cross section to the Coulomb cross section, as a function of the scattering angle, was the experimental quantity of interest here. The yield of counts per microcoulomb of integrated beam at a given angle was normalized

to the most forward angle at which reliable data were obtained and the ratio σ/σ_c taken to be unity at that angle.

In the determination of this quantity for a given scattering angle, the scaler reading and pen-recorder reading of the voltage across the precision capacitor used with the integrating electrometer were made. It was estimated that the values of the capacitors were known to within 1% and the uncertainty in recorder readings to within 0.5%. The fractional standard deviation in counts, taking background into consideration, was combined quadratically with the fractional standard deviation of the value of the integrated beam in order to obtain the uncertainty in σ/σ_c.

As an example, the magnitude of the uncertainty in σ/σ_c for Au at 45°, normalized at 7° (laboratory system) yields a fractional standard deviation of 2.1%. The uncertainties, with respect to both the scattering angle and the ratio σ/σ_c, lie essentially within the area of the circular dots or otherwise indicated limits of uncertainty as shown in the angular distributions.

III. RESULTS

The angular distributions obtained with 48.2-Mev alpha particles elastically scattered from Au, Pb, and Ag are shown in Figs. 7, 8, and 9. The curves shown are theoretical and were derived from the application of a modification of Blair's theory, to be discussed below.

The data for Au show that the cross section dips below and then rises about 3% above that for Coulomb scattering at 20° and then falls exponentially, with slight indications of some structure at 38°, 48°, and 88°. Beyond 100° the cross section is $\sim 10^{-4}$ that for Coulomb scattering. Points were taken every 10° between 120° and 160°, which all lie below the base line of 5×10^{-5}. The points at 160° and 170° indicate a possible rise in the extreme backward direction.

The data for Pb show a similar general behavior, but the maximum rise is to 26% above Coulomb scattering at 20°, and

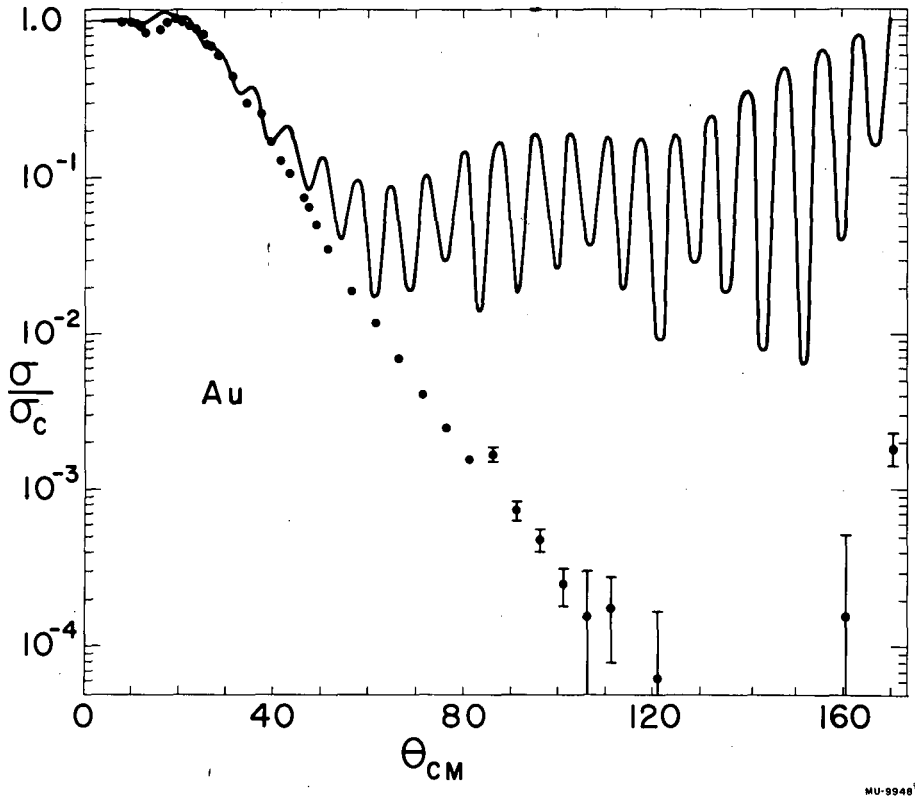

Fig. 7. The angular distribution of 48-Mev alpha particles scattered elastically from Au. The solid curve represents the best fit according to the modified Blair theory. Angles are in degrees.

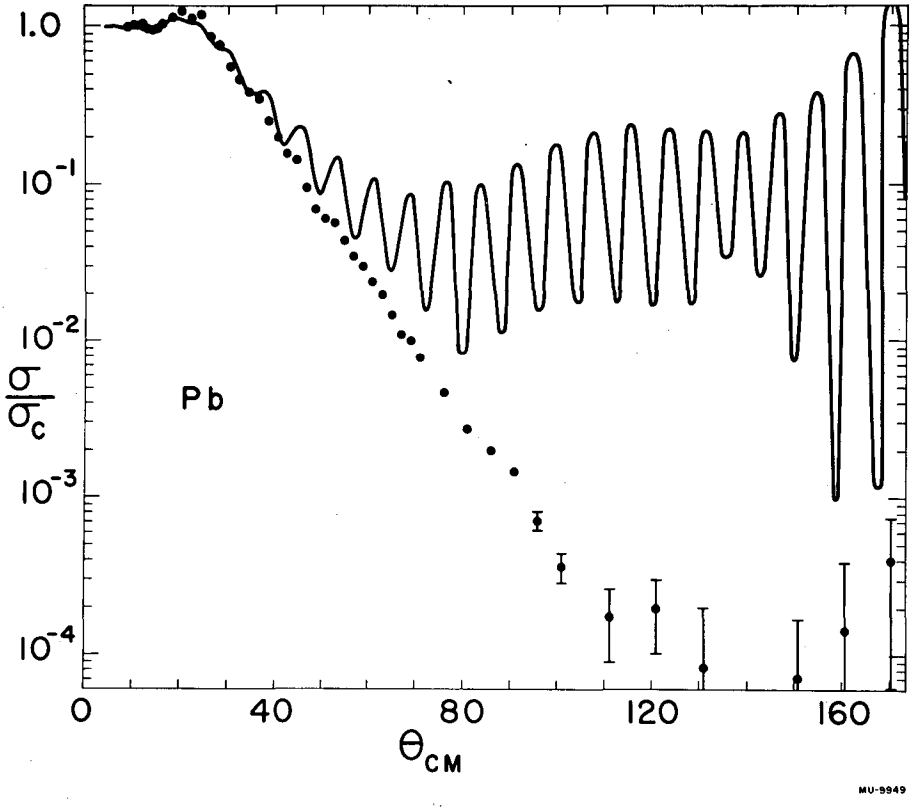

Fig. 8. The angular distribution of 48-Mev alpha particles scattered elastically from Pb. The solid curve represents the best fit according to the modified Blair theory. Angles are in degrees.

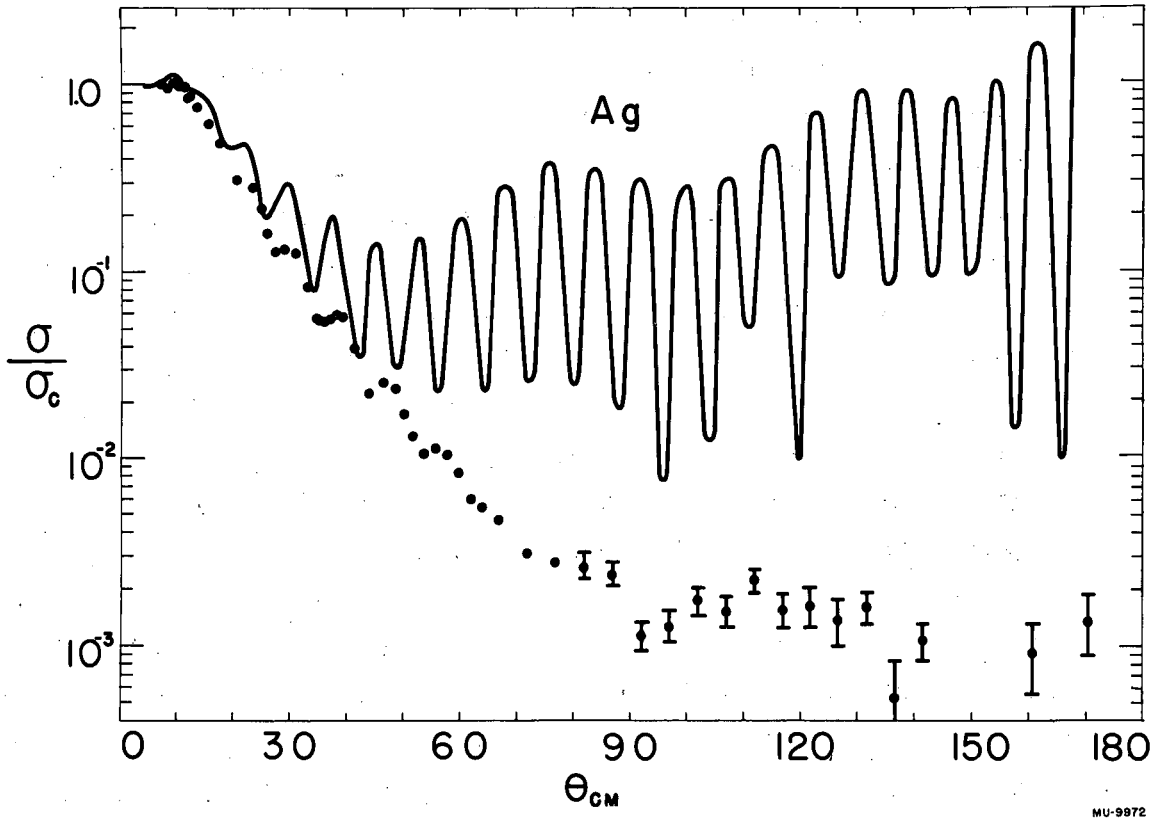

Fig. 9. The angular distribution of 48-Mev alpha particles scattered elastically from Ag. The solid curve represents the best fit according to the modified Blair theory. Angles are in degrees.

definite diffraction maxima may be seen at 38°, 45°, 53°, 70° and 90°. The point at 140° lies below 10^{-4}, and beyond 150° a slight rise in the cross section appears.

The data for Ag show a 2% rise above Coulomb at 10° and the fall-off shows a regular diffraction pattern with distinct maxima at 24°, 30°, 39°, 47°, and 56°. Beyond 90° the cross section remains near 10^{-3} that for Coulomb scattering except for the lower point at 150°.

IV. THEORY AND DISCUSSION

A. The modified Blair theory

The sharp diffraction patterns and relatively high cross sections predicted by Blair's theory, as described in section I, were not observed in these data. On the assumption that this effect is due to the sharp radial cutoff of the theory, it was decided to extend the modification suggested by Wall et al. by weighting the partial-wave amplitudes in such a way as to introduce a broad transition region of interaction. Since $\ell' = f_1(R)$ from Eq. (2), then $\Delta \ell' = f_2(\ell', R)\, \Delta R$. Here ΔR represents a region in which the nuclear density is falling off and has been taken to be equal in magnitude to the alpha-particle radius. Over this region the absorption has been made to decrease linearly. Elsewhere $W_\ell = 1$ (complete absorption) for $\ell \lesssim \ell' - \Delta \ell'$, and $W_\ell = 0$ (no absorption) for $\ell \gtrsim \ell'$. W_ℓ is shown as a function of $\ell / \ell_{c\ell}$ in Fig. 10. The sharp-cutoff model and Wall's modification are shown for comparison. The target elements and alpha-particle energy in this experiment yield a transition region whose magnitude is given by $\frac{\Delta \ell'}{\ell'} \sim 1/3$, or alternatively, $\frac{\Delta R}{R} \sim 1/4$.

In general the introduction of a relatively large transition region causes the theoretical distributions to fall off somewhat faster. The diffraction pattern, however, still appears with the large oscillations characteristic of the sharp-cutoff theory. For the forward angles the curves agree qualitatively with the observed distributions and are sufficiently sensitive to choice of ℓ' that they may be used

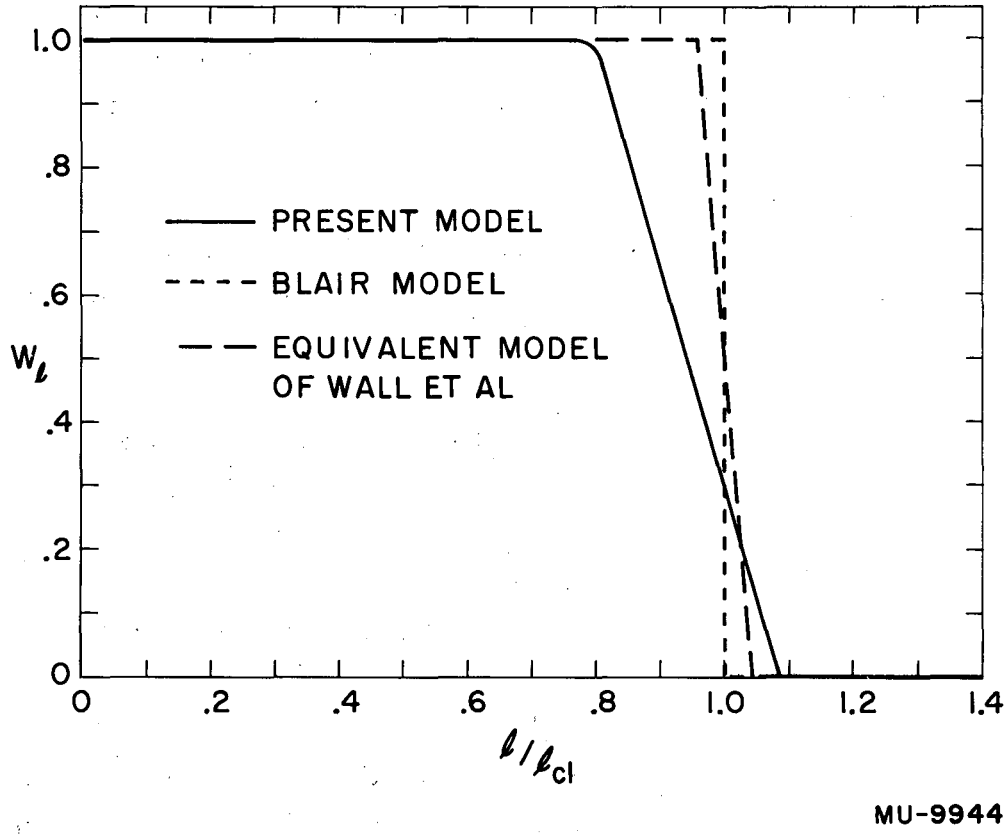

Fig. 10. The weighting factor W_ℓ for removing the ℓth partial wave as a function of $\ell/\ell_{c\ell}$. $\ell_{c\ell}$ is the value of ℓ' which results from Eq. (2).

to determine interaction radii by fitting the curves to the data. Figure 11 shows the effect of changing ℓ' by a small amount. The curves fall more sharply with increasing ℓ'. Figure 11 also compares modified theoretical distributions with a sharp-cutoff distribution for the same target. The modified distribution can be characterized by the parameter ℓ'_{max}, the value of ℓ' for which W_ℓ approaches zero. If the data are fitted with both modified and sharp-cutoff theories, the value of ℓ'_{max} for the modified theory is somewhat larger than the ℓ' for the sharp-cutoff model. Then ℓ'_{max} corresponds to a maximum interaction radius. The fact that even the modified distributions do not drop sharply enough and contain large oscillations is perhaps evidence that a yet larger transition region is required, in contrast with the results at 22 Mev.

B. The Porter theory

Shown in Fig. 12 are plots of the ratio of observed to Coulomb cross sections as a function of the apsidal distance D according to Porter's[6] theory. The curves are those contained in his work and the values of D shown there do not extend to the higher values (up to $D \sim 40 \times 10^{-13}$ cm) which would be necessary for the scattering at angles less than about 15° in the case of Pb or Au bombarded with 48.2-Mev alpha particles.

Choosing $R = R_n + R_\alpha$, with $R_n = 1.5\, A^{1/3} \times 10^{-13}$ cm and $R_\alpha = 1.2 \times 10^{-13}$ cm, we find that the theory reproduces the general features of the data, but the comparison does not here yield unique values of the parameters d and $R/1_o$ which are varied to obtain the curves shown. For Pb and Au, the diffuseness parameter $d = 2 \times 10^{-13}$ cm is a reasonable choice and $R/1_o \sim 3$ or 4 gives best agreement. For Ag, the best value of $R/1_o$ is more uncertain than for Au and Pb, since none of the curves fit the data closely.

C. Interaction radii

Values of the interaction radii have been estimated from the data for this experiment by (a) using the modified version of Blair's theory to obtain the value of ℓ' for which a best fit is obtained and solving for R in Eq. (2); and (b) using Blair's result

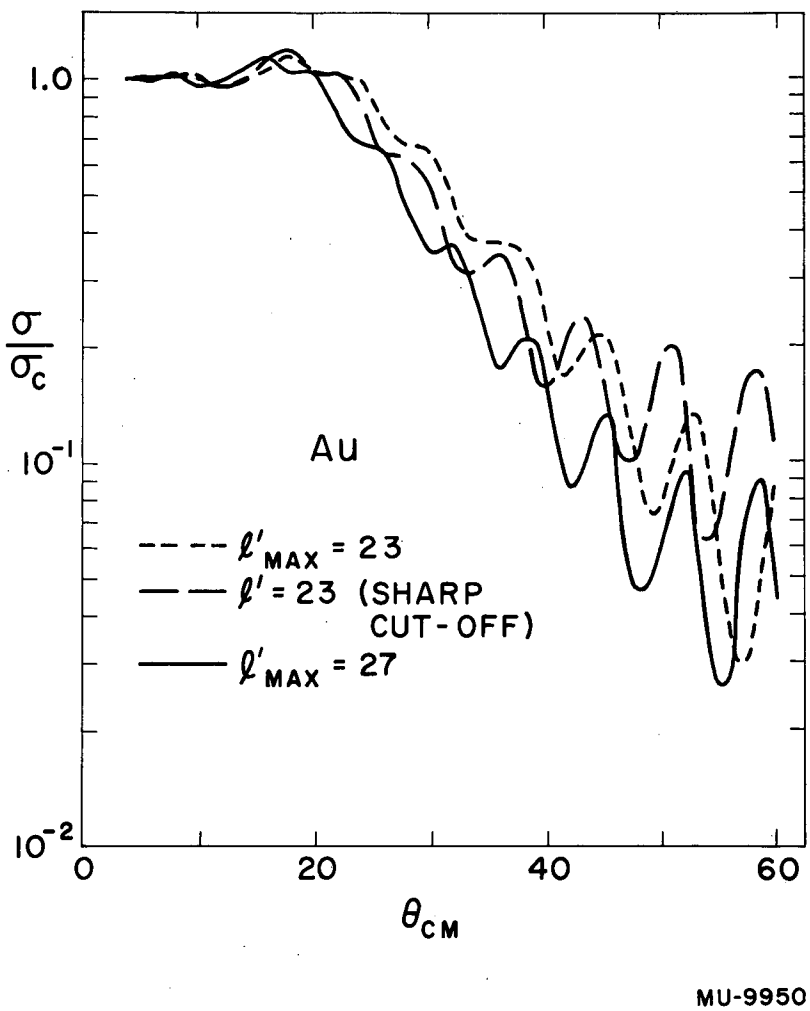

Fig. 11. The dependence of the angular distribution on the value of ℓ'_{max}. Angles are in degrees.

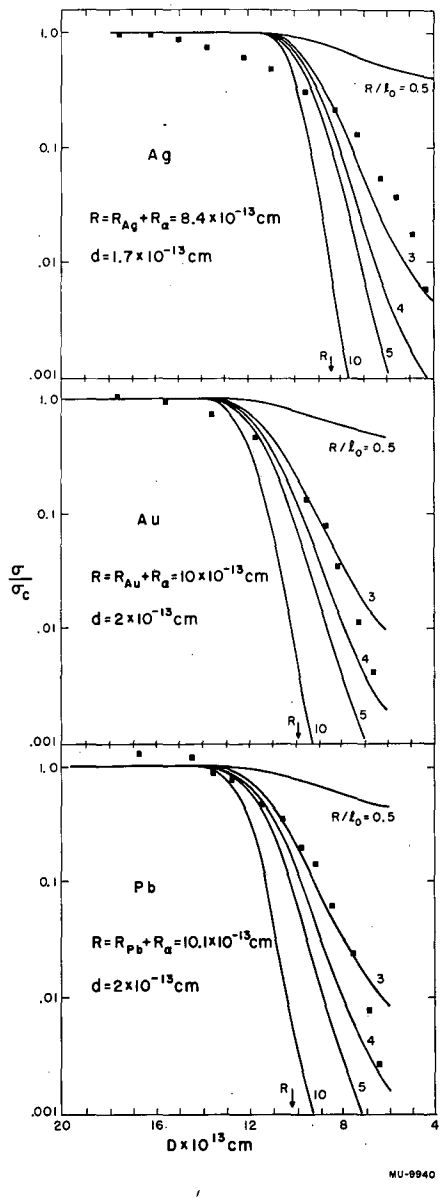

Fig. 12. The angular distributions as a function of D, the apsidal distance, according to Porter's theory. Only a limited number of experimental points are included.

that for a given alpha-particle energy the value of the scattering angle θ, for which the ratio $\sigma/\sigma_c = 1/4$ yields R according to the equation for the apsidal distance

$$D_{1/4} = R = \frac{2Ze^2}{2E}\left(1 + \csc\frac{\theta_{1/4}}{2}\right).$$ Table I lists interaction radii obtained by these methods. The results of other experiments are included for comparison.

The nominal values indicate that the interaction radius for Pb may be slightly smaller than that for Au, in contrast to the results of other experimenters. This may be evidence of a closed-shell configuration in Pb, but the uncertainty in curve fitting and in normalization are sufficiently large that this effect is in doubt. The values obtained here seem to be in general agreement with the other results.

The angular distributions for Au and Pb are very similar, qualitatively. Both sets of data are plotted together in Fig. 13. Wall et al.[5] have explained a similar result obtained at 22 Mev, using a classical interaction model in which the angular distribution depends only on the distance between the alpha particle and the nuclear surface. (see Appendix II for derivation of relation between $R_{Pb} - R_{Au}$ and $\theta_{Pb} - \theta_{Au}$). Under the same assumptions, these data were analyzed to obtain $R_{Pb} - R_{Au}$, and the results, shown in Table II, yield no consistent pattern. The displacement of the two curves, instead of being a smooth function of the angle θ, varies from point to point because of the effects of the differences in the details of structure in the two distributions. The failure occurs probably -- at least in part -- because the criterion for the classical approach, $n >> \ell$, is not well satisfied for $n \sim 7$. An alternative explanation is that the assumptions concerning the interaction are not correct at 48 Mev.

The elastic scattering of medium-energy nucleons has recently been analyzed by several investigators.[9, 12] In applying the optical model of the nucleus it has been found that the parameter representing the nuclear radius has nearly the same value over a wide range of elements. Several of these values have been used to compute interaction radii to be compared with the radii

determined from the data. The results are shown in Table III. The interaction radii determined by method A agree most closely with a nuclear radius given by $R_n = 1.33A^{1/3} \times 10^{-13}$ cm, while the radii determined by method B agree best with

$$R_n = (1.22A^{1/3} + 0.7) \times 10^{-13} \text{ cm.}$$

Preparations have been made to submit the data for analysis on the optical model theory. If the experimental data can be fitted over a wider range of angles by this method, more accurate values of the nuclear parameters that characterize the scattering may be obtained.

Table I

Interaction radii for 48.2-Mev elastically scattered alpha particles. Method A is the Blair one-quarter-point formula. Method B is the fitting of the modified Blair theory to experimental data. Method C is the fitting of the Ford-Wheeler theory to experimental data.

			$R = R_n + R_a$		
Experimenter	E_a(Mev)	Method	Ag	Au	Pb
Washington[3]	13 - 42	A	8.3 ± 0.3	10.05 ± .16	10.26 ± .17
		A		10.45 ± .25	
Indiana[5]	22	B	9.9	11.1	11.4
		A	9.1 ± .3		
Brookhaven[7]	44	B	9.1	10.7	10.9
		C	8.69	10.06	10.20
Berkeley	48.2	A	8.35 ± .28	10.04 ± .20	10.01 ± .19
		B	9.41 ± .17	10.5 ± .2	10.3 ± .2

Table II

Determination of $\Delta R = R_{Pb} - R_{Au}$, in units of 10^{-13} cm.

θ_{Au} = angle of scattering from Au nucleus in degrees.

θ_{Pb} = angle of scattering from Pb nucleus for which $\frac{\sigma}{\sigma_c}$ (Pb, θ_{Pb}) = $\frac{\sigma}{\sigma_c}$ (Au, θ_{Au}). $\Delta\theta = \theta_{Pb} - \theta_{Au}$.

θ_{Au}	$\Delta\theta_{exp}$	$\Delta R = -0.15$	$\Delta R = -0.10$	$\Delta R = -0.05$	$\Delta R = 0$	$\Delta R = 0.05$	$\Delta R = 0.10$	$\Delta R = 0.15$	$\Delta R = 0.20$	$\Delta R = 0.25$
25	3.3	1.6	1.4	1.3	1.2	1.1	0.9	0.8	0.7	0.6
30	2.5	2.0	1.8	1.7	1.5	1.3	1.1	0.9	0.8	0.6
45	2.5	3.8	3.4	3.0	2.5	2.1	1.7	1.3	0.9	0.6
60	5.5	6.2	5.4	4.6	3.8	3.1	2.3	1.5	0.9	0.6
75	5.5	11.7	10.2	8.6	7.4	6.1	4.8	3.6	2.4	1.2
90	4.0	14.5	12.2	9.9	7.9	5.9	4.3	2.3	0.5	---
100	4.0	19.1	15.7	12.7	10.0	7.3	4.8	2.5	0.3	---
120	20	39.7	29.7	22.5	16.4	11.5	7.1	3.0	---	---

Table III

Interaction radii computed from various formulas; R_1 using $1.5\ A^{1/3}$, R_2 using $1.22\ A^{1/3} + 0.7$, and R_3 using $1.33\ A^{1/3}$. R_4 and R_5 were determined from this experiment by Methods A and B, respectively. The alpha-particle radius in each case was computed by the same formula as the nuclear radius. All radii are in units of 10^{-13} cm.

Element	$R_j = R_n + R_a$				
	R_1	R_2	R_3	R_4	R_5
Ag	9.52	9.15	8.44	8.35	9.41
Au	11.11	10.44	9.85	10.04	10.5
Pb	11.27	10.57	9.99	10.01	10.3

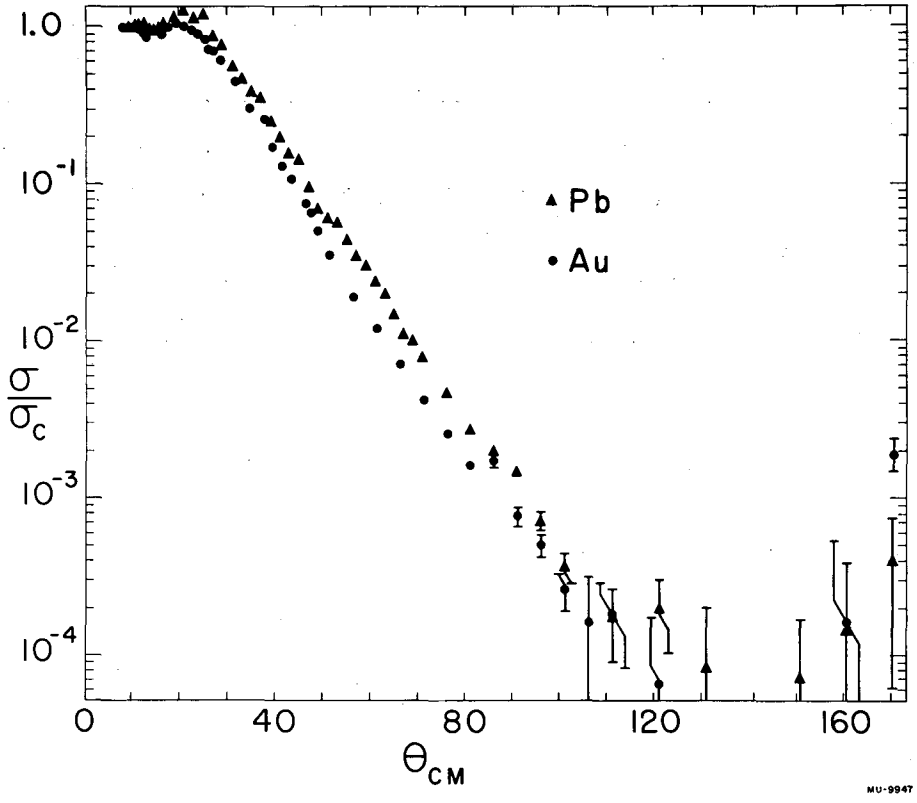

Fig. 13. The angular distributions for Pb and Au plotted together for comparison. Angles are in degrees.

ACKNOWLEDGMENTS

It is a pleasure to thank Prof. A. C. Helmholz for his patient guidance and assistance in the work and to thank Dr. C. M. Van Atta for his interest and support. Dr. Warren Heckrotte has provided many valuable discussions concerning the experiment. Dr. Sidney Fernbach has contributed invaluable time and effort in the Univac program which made the many laborious computations possible. The assistance of Mr. F. Vaughn, Mr. H. Conzett, and Mr. R. Summers-Gill in setting up the cyclotron runs and obtaining the data is gratefully acknowledged. Mr. G. B. Rossi, Mr. W. B. Jones, and the other members of the 60-inch cyclotron group have provided outstanding cyclotron operation for all the runs. For suggesting this problem and for his efforts in all aspects of the work, I am particularly indebted to Dr. Larry Schecter.

APPENDIX I

Derivation of $\frac{\sigma}{\sigma_c}$.

The differential cross section for elastic scattering in terms of partial waves in the center-of-mass system is

$$\sigma = \left| \frac{\lambda\!\!\!^{-}}{2i} \sum_{\ell=0}^{\infty} (2\ell + 1)\,(\eta_\ell - 1)\, P_\ell\,(\cos\,\theta) \right|^2 \qquad (1)$$

where η_ℓ is the coefficient of the outgoing l^{th} wave. For pure Coulomb scattering,

$$\eta_\ell = e^{2i\delta_\ell} = \frac{\Gamma(1 + \ell + in)}{\Gamma(1 + \ell - in)}, \qquad (2)$$

where $n = \frac{ZZ'e^2}{\hbar v}$.

The Coulomb scattering amplitude has been found exactly, and is

$$f(\theta) = \frac{ZZ'e^2}{2Mv^2} \sin^{-2}\frac{\theta}{2}\; e^{-in\ell n \sin^2\frac{\theta}{2} + i\pi + 2i\,\delta_o}.$$

Since

$$\lambda\!\!\!^{-} = \frac{\hbar}{P} \quad \text{and} \quad e^{i\pi} = -1,$$

then

$$f(\theta) = \frac{\lambda\!\!\!^{-}}{2}\left[\frac{-n}{\sin^2\frac{\theta}{2}}\; e^{-in\ell n \sin^2\frac{\theta}{2} + 2i\,\delta_o}\right]. \qquad (3)$$

Alternatively, from Eq. (1),

$$f(\theta) = \frac{\lambda\!\!\!^{-}}{2i} \sum_{\ell=0}^{\infty} (2\ell + 1)\,(\eta_\ell - 1)\, P_\ell(\cos\,\theta)$$

$$= \frac{\lambda\!\!\!^{-}}{2i}\left\{\sum_{\ell=0}^{\infty} -(2\ell+1)\,P_\ell(\cos\theta) + \sum_{\ell=0}^{\ell'} (2\ell+1)\,\eta_\ell P_\ell(\cos\theta) + \sum_{\ell=\ell'+1}^{\infty} (2\ell+1)\,\eta_\ell\, P_\ell(\cos\theta)\right\}.$$

Here the outgoing wave has been represented by the last two terms. Under the assumptions of the Blair model, the second term vanishes owing to the interaction between the alpha particle and the nucleus, and the η_ℓ of the third term are given by Eq. (2). Thus we can write

$$f(\theta) = \frac{\lambda}{2}\left\{-i\left[\frac{-in}{\sin^2\frac{\theta}{2}}\, e^{-in\ell n \sin^2\frac{\theta}{2} + 2i\delta_o} - \sum_{\ell=o}^{\ell'} (2\ell+1)\, e^{2i\delta_\ell} P_\ell(\cos\theta)\right]\right\},$$

which says that the scattered amplitude is just the amplitude for Coulomb scattering, minus the contribution to Coulomb scattering of all outgoing waves up to l'.

Then

$$\sigma = \frac{\lambda^2}{4}\left|\frac{-in}{\sin^2\frac{\theta}{2}}\, e^{-in\ell n \sin^2\frac{\theta}{2} + 2i\,\delta_o} - \sum_{\ell=o}^{\ell'} (2\ell+1)\, e^{2i\delta_\ell} P_\ell(\cos\theta)\right|^2 .$$

Taking out the factor $e^{2i\delta_o}$, we have

$$\sigma = \frac{\lambda^2}{4}\left|e^{2i\,\delta_o}\left\{\frac{-in}{\sin^2\frac{\theta}{2}}\, e^{-in\ell n \sin^2\frac{\theta}{2}} - \sum_{\ell=o}^{\ell'} (2\ell+1)\, e^{2i(\delta_\ell - \delta_o)} P_\ell(\cos\theta)\right\}\right|^2,$$

and dividing by

$$\sigma_c = \frac{\lambda^2}{4}\,\frac{n^2}{\sin^4\frac{\theta}{2}},$$

the Coulomb differential scattering cross section, we get

$$\frac{\sigma}{\sigma_c} = \left| -ie^{-in\ell n \sin^2\frac{\theta}{2}} - \frac{\sin^2\frac{\theta}{2}}{n}\sum_{\ell=o}^{\ell'} (2\ell+1)\, e^{2i(\delta_\ell - \delta_o)} P_\ell(\cos\theta)\right|^2 .$$

If we wish to weight the probability of eliminating the lth wave ($l \leq l'$), we write

$$\frac{\sigma}{\sigma_c} = \left| -ie^{-in\ell n \sin^2\frac{\theta}{2}} - \frac{\sin^2\frac{\theta}{2}}{n}\sum_{\ell=o}^{\ell'} (2\ell+1)\sqrt{w}_\ell\, e^{2i(\delta_\ell - \delta_o)} P_\ell(\cos\theta)\right|^2 .$$

The phase factors are given by

$$e^{2i\delta_\ell} = \frac{\Gamma(1+\ell+in)}{\Gamma(1+\ell-in)} = \frac{(\ell+in)!}{(\ell-in)!} = \frac{(\ell+in)(\ell-1+in)!}{(\ell-in)(\ell-1-in)!} = \frac{\ell+in}{\ell-in}\,\frac{\Gamma(\ell+in)}{\Gamma(\ell-in)} = \frac{\ell+in}{\ell-in}\, e^{2i\delta_{\ell-1}} .$$

Hence,

$$e^{2i(\delta_\ell - \delta_o)} = \frac{\ell+in}{\ell-in}\, e^{2i(\delta_{\ell-1} - \delta_o)} .$$

APPENDIX II

Determination of $R_{Pb} - R_{Au}$

If the ratio $\frac{\sigma}{\sigma_c}$ depends only on the distance between the alpha particle trajectory and the nuclear surface, then letting the subscripts 1 and 2 refer to Au and Pb, respectively,

$$\frac{\sigma_1(\theta_1)}{\sigma_c(\theta_1)} \doteq \frac{\sigma_2(\theta_2)}{\sigma_c(\theta_2)} \tag{1}$$

if

$$D_1 - R_1 = D_2 - R_2 \ . \tag{2}$$

Since

$$\frac{P}{\hbar} D = n\left(1 + \frac{1}{\sin\frac{\theta}{2}}\right) = n f(\theta), \tag{3}$$

then (2) becomes

$$n_2 f(\theta_2) = n_1 f(\theta_1) + \frac{P}{\hbar}(R_2 - R_1). \tag{4}$$

For various assumptions about $\Delta R = R_2 - R_1$, $\Delta\theta = \theta_2 - \theta_1$ has been computed from equation (4). From Fig. 13 $\Delta\theta_{exp}$ has been estimated for a series of points as the difference in angle θ for which the Au and Pb distributions satisfy equation (1). The results are given in Table II.

References

1. E. Rutherford, Phil. Mag. 21, 669 (1911); H. Geiger and E. Marsden, Proc. Roy. Soc. (London) A82, 495 (1909); H. Geiger and E. Marsden, Phil. Mag. 25, 604 (1913); J. Chadwick, Phil. Mag. 40, 734 (1920); E. Rutherford and J. Chadwick, Phil. Mag. 50, 889 (1925).
2. For example, see J. M. Blatt and V. F. Weisskopf, "Theoretical Nuclear Physics" (John Wiley and Sons, Inc., New York, 1952) p. 317.
3. G. W. Farwell and H. E. Wegner, Phys. Rev. 95, 1212 (1954).
4. J. S. Blair, Phys. Rev. 95, 1218 (1954).
5. N. S. Wall, J. R. Rees, and K. W. Ford, Phys. Rev. 97, 726 (1955).
6. C. E. Porter, to be published.
7. H. E. Wegner, R. M. Eisberg, and G. Igo, to be published.
8. For example, see Conference, Brookhaven National Laboratory (January 1955) on "Statistical Aspects of the Nucleus."
9. M. A. Melkanoff, J. S. Nodvik, D. S. Saxon, and R. Woods, Technical Report 7-12-55, Dept. of Physics, UCLA.
10. G. E. Fischer, Phys. Rev. 96, 704 (1954).
11. B. B. Rossi and H. H. Staub, "Ionization Chambers and Counters, Experimental Techniques" (McGraw-Hill Book Co., Inc., New York, 1949) p. 96.
12. S. Fernbach, private communication.